Materials Research. 2018; 21(5): e20170992.
DOI: http://dx.doi.org/10.1590/1980-5373-MR-2017-0992

The Microstructure and Mechanical Properties of As-cast Mg-10Gd-3Y-xZn-0.6Zr (x = 0, 0.5, 1 and 2 wt%) Alloys

***Zhibing Ding*[a,b], *Ruopeng Lu*[a], *Yuhong Zhao*[a]*, *Hua Hou*[a], *Peng Cheng*[a], *Bu Zhiqiang*[a], *Peilin Zhang*[a]**

[a]*College of Materials Science and Engineering, North University of China, Taiyuan 030051, China*
[b]*College of Mechatronic Engineering, North University of China, Taiyuan 030051, China*

Received: November 08, 2017; Revised: May 10, 2018; Accepted: May 22, 2018

The microstructure, mechanical properties and fracture behavior of as-cast Mg-10Gd-3Y-xZn-0.6Zr (x = 0, 0.5, 1 and 2 wt%) alloys have been investigated by X-ray diffraction (XRD), optical microscopy (OM), scanning electron microscopy (SEM) and tensile tests. The experimental results reveal that the microstructure of the alloy without Zn contains α-Mg and $Mg_{24}(Gd,Y)_5$ phase, the microstructure of the alloy with 0.5% Zn contained of α-Mg, $(Mg,Zn)_3(Gd,Y)$ and $Mg_{24}(Gd,Y,Zn)_5$ phase, whereas when Zn content was 1% and 2%, the $Mg_{12}(Gd,Y)Zn$ phase and some needle-shaped stacking faults notably appear and the $Mg_{24}(Gd,Y,Zn)_5$ phases completely disappear. Moreover, a new 18R long period stacking ordered (LPSO) phase is observed in grain boundaries with increasing Zn content up to 2%. The tensile tests indicate that the alloy containing 0.5% Zn shows the optimal mechanical properties and the ultimate tensile strength (UTS), yield strength (YS) and elongation are 228MPa, 172MPa and 5.1%, respectively. As indicated by fracture analyses, the fracture modes of the alloys with 0%, 1% and 2% Zn are brittleness transcrystalline fracture, and the tensile fracture mode of 0.5% Zn alloy is typical tough transgranular fracture.

Keywords: *Microstructure, Stacking fault, LPSO phase, Mechanical properties.*

1. Introduction

As the lightest metallic structural materials, magnesium alloys have drawn great attention recently. Magnesium alloys are of great potential to be used in the aerospace, military, biomedical devices and automotive industries because of their low density, high specific strength, and excellent machinability[1-4]. The existing commercial magnesium alloys for automotive applications are AZ91D (Mg-9Al-0.7Zn), AM50A (Mg-5Al-0.4Mn) and AM60B (Mg-6Al-0.4Mn). These alloys have an excellent combination of corrosion resistance and die castability[5,6]. However, their low mechanical properties cannot meet the current requirements of the civilian industries especially at high temperature.

It was reported that the addition of RE (rare-earth) element to magnesium alloys can improve creep properties than conventional Mg-Al alloys, and the most prominent alloys are Mg-Gd-Y-Zr series[7-9]. The addition of Zn to the Mg-Gd-Y-Zr alloys can significantly improve the strengthening of the alloy, and different types of long periodic stacking ordered (LPSO) structures can easily observe during homogenization treatment in many Mg-RE-Zn series[10-12]. $Mg_{97}Zn_1Y_2$ (at.%) was developed using rapidly solidified powder metallurgy in 2001. It is a novel alloy with superior mechanical properties including tensile yield strength of 6l0MPa and elongation of 5%. The main reason for the excellent mechanical properties of these alloys is that the existence of LPSO structure improves the hardness and strength of magnesium alloys[13,14]. The LPSO phase consists of a solid solution of Y and Zn in a magnesium matrix where these atoms are placed periodically in the magnesium basal planes forming an ordered structure[15]. It is very interesting that such small additives like 1-3 at.% Zn and Y into pure Mg can change dramatically its microstructure and mechanical properties.

Many investigations related to the microstructure and mechanical properties of the Mg-Gd-Y-Zn-Zr system have been reported[16-18]. Nevertheless, the formation mechanism of LPSO structure still remains unclear until now. Accordingly, the aim of the present paper is to systematically study the influence of Zn concentration on the microstructure and mechanical properties of as-cast Mg-10Gd-3Y-0.6Zr (wt%) alloys.

2. Experimental Procedures

To obtain as-cast Mg-10Gd-3Y-xZn-0.6Zr (x = 0, 0.5, 1 and 2 wt%) alloys, Mg-30%Gd, Mg-30%Y, Mg-30%Zr master alloys, pure Mg and Zn were melted in an medium frequency induction heating furnace using a small steel crucible with a diameter of 98 mm under a protective argon atmosphere at 780°C. The melt was cooled in water after adequate stirring.

*e-mail: zhaoyuhong@nuc.edu.cn

The chemical compositions of the alloys were determined by inductively coupled plasma spectroscopy and are listed in Table 1. The samples for optical microscope (OM) and scanning electron microscope (SEM) analyses are prepared by the standard technique of grinding with SiC abrasive paper and polishing with an MgO suspension solution, followed by etching in a 4vol% nital solution. Phase analysis is conducted using a Rigaku D/MAX2500PC X-ray diffractometer with a copper target at scanning angles from 20º to 90º and scanning speed of 5º/min. The detailed microstructure of the samples was further analyzed using a TEM (JEM-2100F) operated at an accelerating voltage of 200 kV.

Tensile tests of above mentioned alloys are performed at a crosshead speed of 1.5mm/min, according to the relevant standard of using cylindrical specimen with marked dimension of 25mm gauge length and 5mm diameter. All tensile tests are carried out on a Zwick/Roell Z020 tensile testing machine. An average of three measurements was used. The tensile fracture surfaces are examined by SEM.

3. Results and Discussion

3.1 Microstructures

Fig. 1 shows the XRD patterns of the as-cast Mg-10Gd-3Y-xZn-0.6Zr alloys. It can be observed that the 0Zn alloys are mainly composed of α-Mg and $Mg_{24}(Gd,Y)_5$ phase. However, in the 0.5Zn alloys, the microstructure is mainly composed of α-Mg, $Mg_{24}(Gd,Y,Zn)_5$ and $(Mg,Zn)_3(Gd,Y)$ phases. In addition, the $Mg_{12}(Gd,Y)Zn$ phases in the 1Zn and 2Zn alloys notably appear and the $Mg_{24}(Gd,Y,Zn)_5$ phases completely disappear. As seen in Fig. 1, the intensity of the diffraction peaks corresponding to $Mg_{12}(Gd,Y)Zn$ phase are strengthened with increasing the amount of Zn addition.

Fig. 2 shows the optical micrographs of the as-cast Mg-10Gd-3Y-xZn-0.6Zr alloys. The as-cast alloys are composed of α-Mg and eutectics distributing along the grain boundaries discontinuously. The grain sizes of these alloys are relatively small because the melt were cooled quickly in water, the average grain sizes of the 0, 0.5, 1 and 2Zn alloys are 34.6, 37.2, 41.7 and 39.5μm, respectively. The high-magnification microstructures of the four alloys are shown in Fig. 2b, d, f and h. As is seen, the secondary phases in all the four alloys are distributed homogeneously in the observed region and

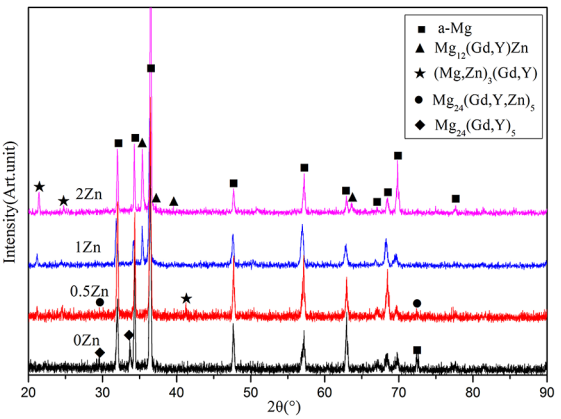

Figure 1. X-ray diffraction patterns of the 0Zn, 0.5Zn, 1Zn and 2Zn alloys alloys.

the block-shaped phase gets coarsened with the increase of Zn elements. It is interesting that some needle-shaped phases can be observed near grain boundaries in 1Zn and 2Zn alloys.

Fig. 3 shows the SEM back-scattered electron (BSE) images of the secondary phase in the as-cast Mg-10Gd-3Y-xZn-0.6Zr alloys. In the 0Zn (Fig. 3a) and 0.5Zn (Fig. 3b) alloys, the bright gray eutectic compounds distribute in grain boundaries in the form of skeleton-shape. On the other hand, the most of the secondary phases are mainly distributed along the grain boundaries with a hollow-out skeleton morphology in the 1Zn (Fig. 3c) and 2Zn (Fig. 3d) alloys, especially 2Zn alloy.

The SEM-EDS results of the four alloys are shown in Fig. 3 and Table 2. Fig. 3a and Table 2 show the SEM-EDS results in the 0Zn alloy. According to XRD and EDS results, it is inferred that the B phase is $Mg_{24}(Gd,Y)_5$. The SEM-EDS results of individual phase in the 0.5Zn alloy are shown in Fig. 3b and Table 2. The content of Zn elements in C phase is higher than that in B phase. It is inferred that the B phase is $Mg_{24}(Gd,Y,Zn)_5$ and the C phase is $(Mg,Zn)_3(Gd,Y)$. The small white square D phase can be determined to be rich in Gd and Y elements. The SEM-EDS results of the 1Zn alloy are displayed in Fig. 3c and Table 2. Combined with microstructure observation and other investigation[19], it can be regarded that the intermetallic eutectic compound B with hollow-out skeleton shape is $(Mg,Zn)_3(Gd,Y)$. The C phase in network-shape possess an approximate composition of 90.30Mg-4.58Gd-2.09Y-3.04Zn which is close to the

Table 1. Actual chemical compositions of Alloys.

Alloy No.	Composition	
	wt%	at%
0Zn	Mg-10.03Gd-3.04Y-0.63Zr	$Mg_{97.16}Gd_{1.73}Y_{0.92}Zr_{0.19}$
0.5Zn	Mg-10.10Gd-2.98Y-0.53Zn-0.61Zr	$Mg_{96.95}Gd_{1.74}Y_{0.91}Zn_{0.22}Zr_{0.18}$
1Zn	Mg-10.05Gd-3.05Y-0.98Zn-0.59Zr	$Mg_{96.74}Gd_{1.74}Y_{0.93}Zn_{0.41}Zr_{0.18}$
2Zn	Mg-10.13Gd-3.12Y-2.03Zn-0.60Zr	$Mg_{96.22}Gd_{1.76}Y_{0.95}Zn_{0.89}Zr_{0.18}$

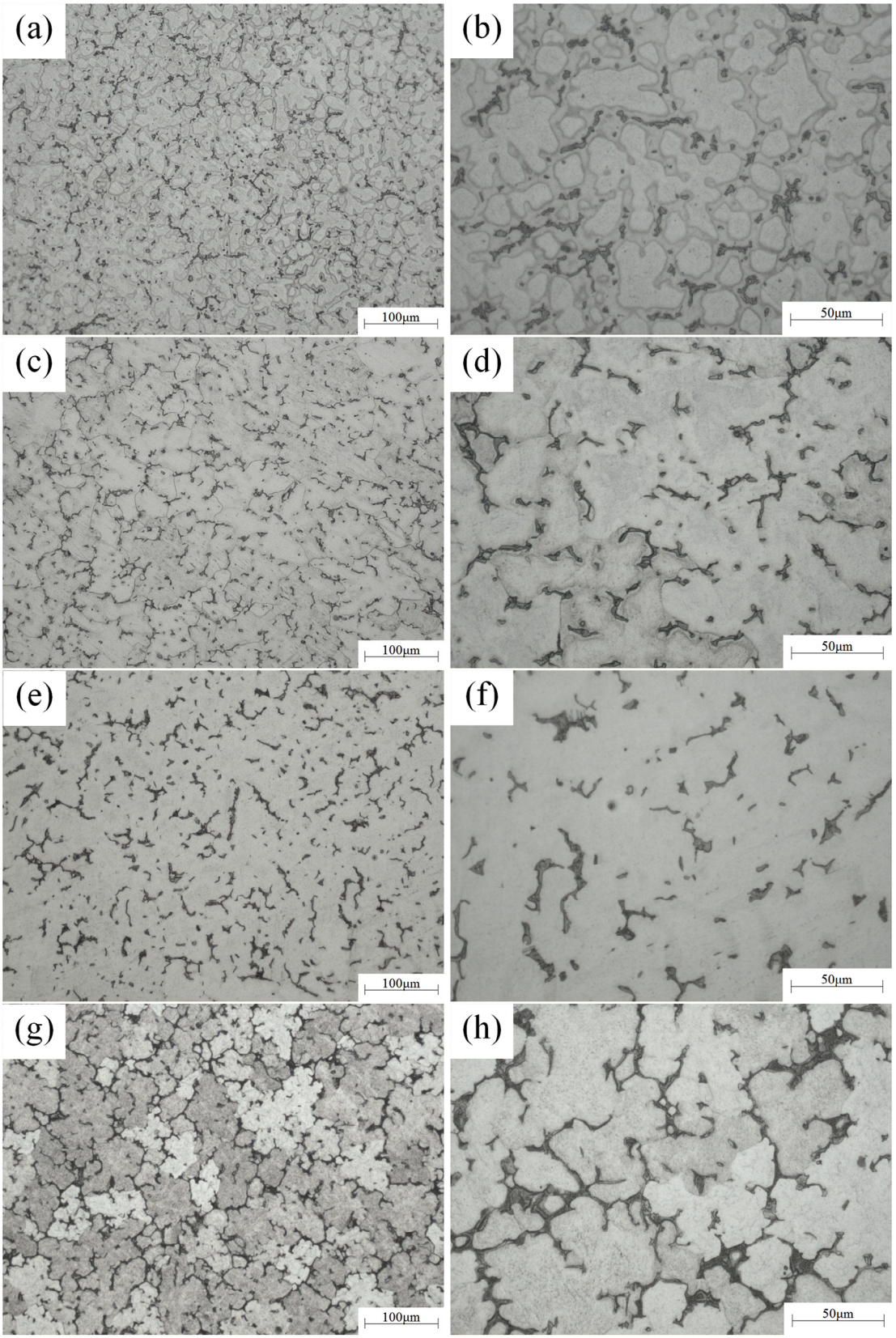

Figure 2. The microstructures of as-cast alloys. (a), (c), (e) and (g) are the low-magnification microstructures of the 0Zn, 0.5Zn, 1Zn and 2Zn alloys, respectively. (b), (d), (f) and (h) are the high-magnification microstructures of the 0Zn, 0.5Zn, 1Zn and 2Zn alloys, respectively.

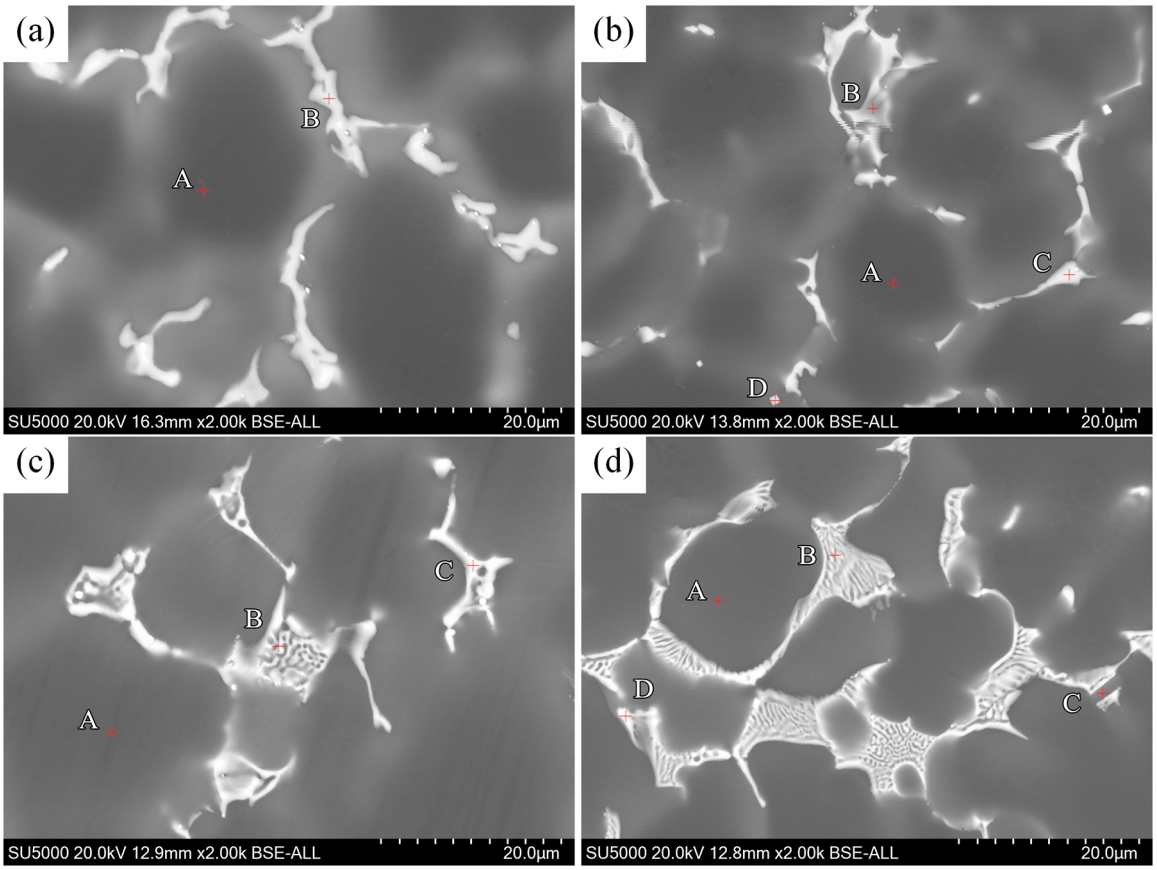

Figure 3. High magnification back scattered electron (BSE) SEM images of the as-cast alloys with different Zn contents: (a) 0%, (b) 0.5%, (c) 1%, (d) 2%. The EDS results are shown in Tables 2.

Table 2. EDS analysis of the selected points in Fig. 3.

Alloys	Positions	wt%				at%				Possible compound
		Mg	Gd	Y	Zn	Mg	Gd	Y	Zn	
0Zn alloy	A	79.19	17.13	3.68	/	95.59	3.20	1.22	/	α-Mg
	B	63.20	30.86	5.94	/	90.81	6.86	2.33	/	$Mg_{24}(Gd,Y)_5$
0.5Zn alloy	A	86.24	10.76	2.64	0.15	97.25	1.87	0.81	0.06	α-Mg
	B	68.59	23.67	4.43	3.32	91.83	4.90	1.62	1.65	$Mg_{24}(Gd,Y,Zn)_5$
	C	63.27	26.40	5.66	4.68	89.57	5.78	2.19	2.46	$(Mg,Zn)_3(Gd,Y)$
	D	26.24	38.71	34.31	0.73	62.66	14.29	22.40	0.65	Enrichment of Gd and Y elements
1Zn alloy	A	83.98	11.70	3.00	1.32	96.42	2.08	0.94	0.56	α-Mg
	B	54.53	30.46	6.60	8.41	84.97	7.34	2.81	4.88	$(Mg,Zn)_3(Gd,Y)$
	C	66.53	21.83	5.62	6.02	90.30	4.58	2.09	3.04	$Mg_{12}(Gd,Y)Zn$
2Zn alloy	A	83.89	11.28	2.79	2.05	96.25	2.00	0.87	0.87	α-Mg
	B	57.87	25.70	5.48	10.96	85.84	5.89	2.22	6.04	$(Mg,Zn)_3(Gd,Y)$
	C	64.64	21.79	5.64	7.93	89.16	4.65	2.13	4.07	$Mg_{12}(Gd,Y)Zn$
	D	60.64	23.53	5.81	10.03	87.13	5.23	2.28	5.36	$Mg_{12}(Gd,Y)Zn$

$Mg_{12}(Gd,Y)Zn$, preliminarily indicating that the phase is a LPSO phase. The SEM-EDS results of individual phase in the 2Zn alloy are shown in Fig. 3d and Table 2, according to XRD and EDS results, the eutectics C and D in the 2Zn alloy belong to the same phase, similar to 1Zn alloy.

It is noted that the second phase in the 0Zn alloy is $Mg_{24}(Gd,Y)_5$, while $Mg_{24}(Gd,Y,Zn)_5$ and $(Mg,Zn)_3(Gd,Y)$ second phases are observed in the 0.5Zn alloy. It is interesting that only $(Mg,Zn)_3(Gd,Y)$ and $Mg_{12}(Gd,Y)Zn$ second phases appear in the 1Zn and 2Zn alloy. EDS results suggest that the Zn content in $(Mg,Zn)_3(Gd,Y)$ is higher than in $Mg_{24}(Gd,Y,Zn)_5$, with no Zn element in the $Mg_{24}(Gd,Y)_5$ phase. As a result, increasing the Zn content leads to the transformation of eutectic phases following the order of $Mg_{24}(Gd,Y)_5 \rightarrow Mg_{24}(Gd,Y,Zn)_5 + (Mg,Zn)_3(Gd,Y) \rightarrow (Mg,Zn)_3(Gd,Y) + Mg_{12}(Gd,Y)Zn$.

Fig. 4a-b shows the bright-field TEM image and SAED patterns of the needle-shaped phase in the 1Zn and 2Zn alloys. The needle-shaped phase with a width of several nanometers are parallel to each other. Being viewed along $<11\bar{2}0>_\alpha$, the light streaks appeared between diffraction spots of α-Mg in SAED patterns demonstrate these line contrasts are stacking faults on $(0001)_\alpha$ basal planes, which is consistent to reports[20,21]. The difference is that the needle-shaped stacking faults in 2Zn alloy is more dense than the 1Zn alloy.

Fig. 5 shows a bright-field image and the corresponding SAED pattern of the LPSO phases in the 2Zn alloy. It is obvious from the corresponding selected area electron diffraction (SAED) patterns that five extra diffraction spots occur at the intervals between $(000)_{18R}$ and $(0018)_{18R}$ spots, which further demonstrates the existence of LPSO phase is 18R (a = 0.325 nm and c = 3.694 nm)[22-25]. In addition, the orientation relationships between 18R and α-Mg phases could also be confirmed as $(001)_{18R}//(0001)_\alpha$ and $[010]_{18R}//[11\bar{2}0]_\alpha$ from the SAED patterns, which is consistent with previous reports[26].

It is obvious that the needle-shaped phases in the 1Zn and 2Zn alloys are not LPSO phases but stacking faults. Suzuki et al.[27] reported that the simultaneous addition of Zn and Y elements in Mg alloy can decrease the stacking fault energy of α-Mg phase on basal plane effectively, which is favorable to the formation of stacking fault. In addition, there are some evidences suggest that the formation of LPSO phase is related to the stacking fault. First, the stacking faults contain structure units with f.c.c. structure stacking sequence[26,28], the formation of 6H, 10H, 14H, 18R and 24R LPSO phases also results in the local structure units with f.c.c. structure stacking order sequence. Second, the stacking fault can cause weak extra streaks and spots in SEAD patterns, which is consistent with 10H, 14H and 18R LPSO phases[26,28,29], these weak extra streaks and spots correspond to the ordering of RE and Zn atoms with several atom layers. Third, the stacking fault exclusively forms in the alloy with low Zn content, whereas high Zn content leads to the formation of stacking fault as well as LPSO phase.

3.2 Mechanical properties

3.2.1 Tensile properties

The tensile properties at RT of the alloys are shown in Fig. 6. The UTS, YS and elongation of the 0Zn alloy are 204MPa, 154MPa, and 3.7%, respectively. The mechanical properties of the 0.5Zn alloy are better than that of other three alloys, and the UTS, YS and elongation are 228MPa, 172MPa and 5.1%, respectively. The UTS, YS and elongation of the 1Zn alloy are 205MPa, 156MPa and 4.4%, respectively. The UTS, YS and elongation are 215MPa, 164MPa and 4.2% for the 2Zn alloy, respectively.

Compared to the alloys with Zn, the mechanical properties of the 0Zn alloy are the lowest. The mechanical properties are mainly determined by eutectic phases, stacking fault, LPSO phase, and grain size. It is well known that any one hard and fragile phase has duality for strengthening role: a good strengthening effect can be achieved if this phase uniformly distributed in small particle form, or a harmful role will generate if it is in coarse particles or continuous

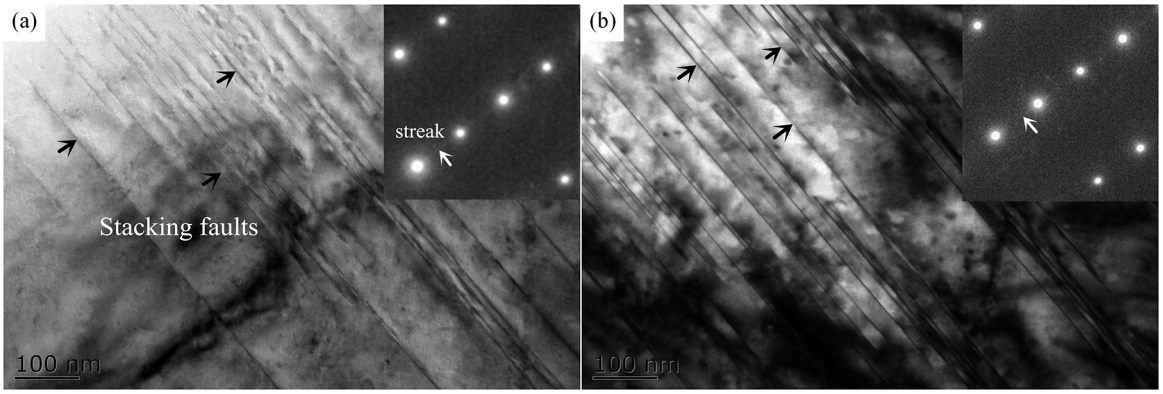

Figure 4. Bright-field TEM image and the corresponding SAED patterns along $<11\bar{2}0>_\alpha$ direction of the needle-shaped phase in 1Zn (a) and 2Zn (b) alloys.

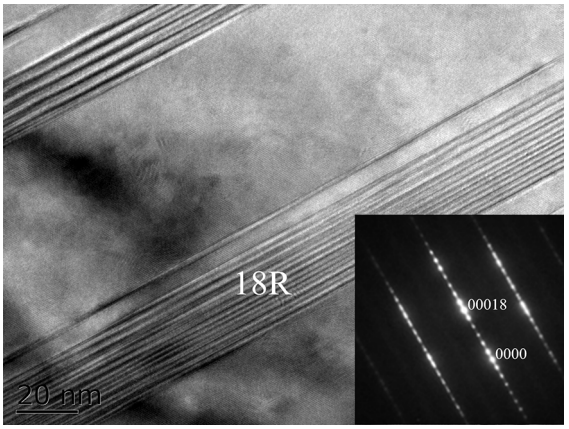

Figure 5. Bright-field TEM image and the corresponding SAED pattern along $<11\bar{2}0>_{\alpha}$ direction of the LPSO phases in the as-cast 2Zn alloy.

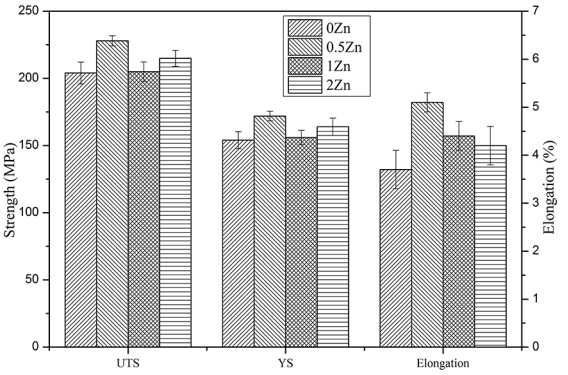

Figure 6. The mechanical properties of the 0Zn, 0.5Zn, 1Zn and 2Zn alloys.

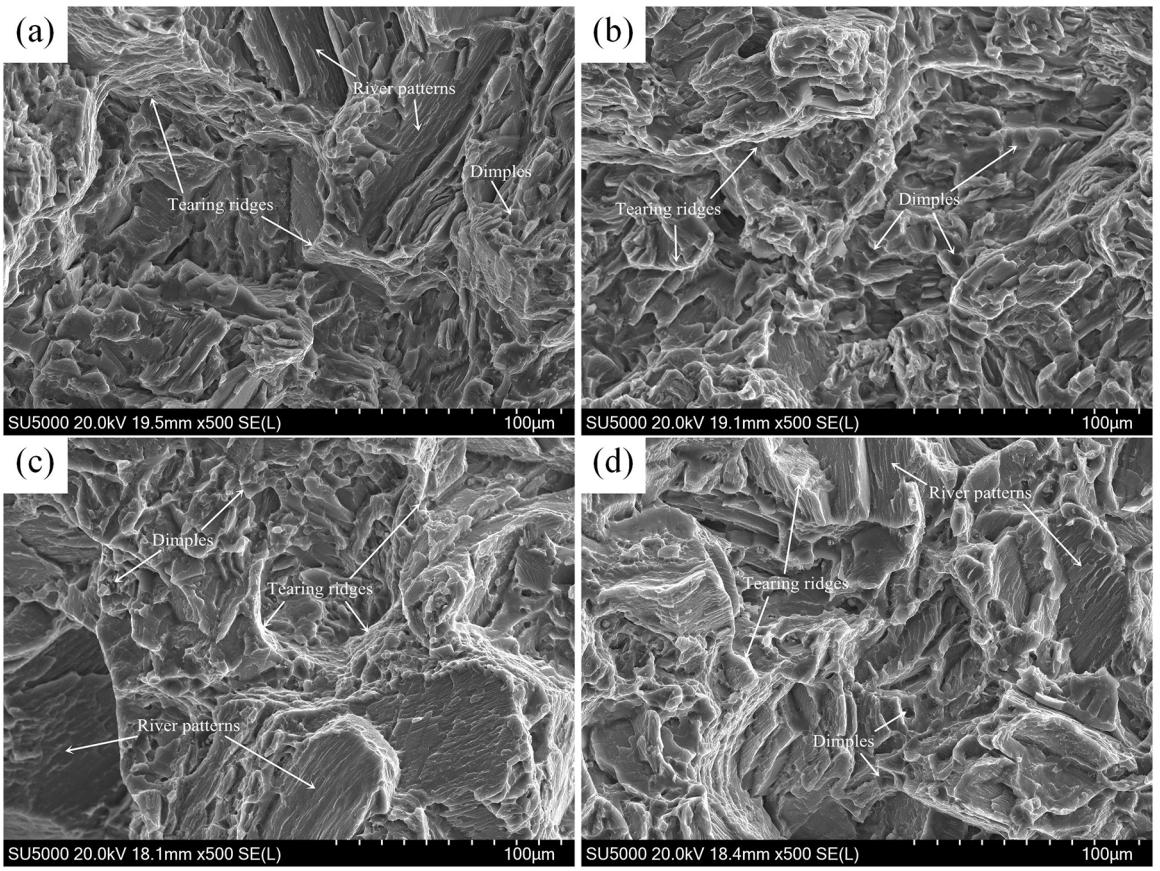

Figure 7. The tensile fracture of the as-cast alloys. (a), (b), (c) and (d) are the SEM images of the fracture surface of the 0Zn, 0.5Zn, 1Zn and 2Zn alloys, respectively.

network shape. Moreover, the present result is consistent to these investigations. Although the LPSO phase has higher elastic moduli and vickers hardness, which can hinder the movement of dislocation, and significantly improve the strength and plasticity of the alloys[3,19]. The hollow-out skeleton $(Mg,Zn)_3RE$ phase has hard and fragile characteristics, and the $(Mg,Zn)_3RE$/α-Mg interfaces are not coherent[30]. Furthermore, the coarse eutectic $(Mg,Zn)_3(Gd,Y)$ phase in grain boundaries can easily cause stress concentration during deformation and thus damage mechanical properties, just like 1Zn and 2Zn alloys.

3.2.2 Fractography

Fig. 7 shows the fracture surfaces of the tensile samples of the as-cast Mg-10Gd-3Y-xZn-0.6Zr alloys. It is observed that there are some dimples, tearing ridges and evident river patterns in the fracture surfaces of 0Zn (Fig. 5a), 1Zn (Fig. 5c) and 2Zn (Fig. 5d) alloys, which indicates that the tensile fracture mode belongs to brittleness transcrystalline fracture. Comparatively, there are mainly dimples with different depths and a few tearing ridges observed in the fracture surfaces of 0.5Zn (Fig. 5b) alloy due to the formation of a small amount of $(Mg,Zn)_3RE$ phases, which is in accordance with its high elongation of 5.1%. This indicates that the tensile fracture mode of 0.5Zn alloy is typical tough transgranular fracture.

4. Conclusions

The microstructure, mechanical properties and fracture behavior of as-cast Mg-10Gd-3Y-xZn-0.6Zr (x = 0, 0.5, 1 and 2 wt%) alloys have been investigated. The conclusions are summarized as follows:

1. The microstructures for the as-cast alloy without Zn is mainly composed of α-Mg and $Mg_{24}(Gd,Y)_5$ phase. However, in the 0.5Zn alloy, the microstructure is mainly composed of α-Mg, $Mg_{24}(Gd,Y,Zn)_5$ and $(Mg,Zn)_3(Gd,Y)$ phases. In addition, the $Mg_{12}(Gd,Y)$ Zn phases in the 1Zn and 2Zn alloys notably appear and the $Mg_{24}(Gd,Y,Zn)_5$ phases completely disappear.
2. TEM analyses indicate that the needle-shaped phase near grain boundary in the 1Zn and 2Zn alloys are stacking faults. The new 18R LPSO phase is observed in the 2Zn alloys.
3. The tensile tests indicate that the Mg-10Gd-3Y-0.5Zn-0.6Zr alloy with a small amount of $(Mg,Zn)_3RE$ phases shows the optimal mechanical properties and the ultimate tensile strength (UTS), yield strength (YS) and elongation are 228MPa, 172MPa and 5.1%, respectively.
4. The tensile fracture modes of the alloys with 0%, 1% and 2% Zn are brittleness transcrystalline fracture, and the tensile fracture mode of 0.5% Zn alloy is typical tough transgranular fracture.

5. Acknowledgments

This work is supported by the National Natural Science Foundation of China (Nos.51774254, 51774253, 51701187, U1610123, 51674226, 51574207, 51574206), The Science and Technology Major Project of Shanxi Province (No. MC2016-06), Shanxi Province Science Foundation for Youths (No.201601D021062).

6. References

1. Liu WC, Jiang LK, Cao L, Mei J, Wu GH, Zhang S, et al. Fatigue behavior and plane-strain fracture toughness of sand-cast Mg-10Gd-3Y-0.5Zr magnesium alloy. *Materials & Design*. 2014;59:466-474.

2. Zhao ZD, Chen Q, Chao HY, Huang SH. Microstructural evolution and tensile mechanical properties of thixoforged ZK60-Y magnesium alloys produced by two different routes. *Materials & Design*. 2010;31(4):1906-1916.

3. Cheng P, Zhao YH, Lu RP, Hou H, Bu ZQ, Yan F. Effect of Ti addition on the microstructure and mechanical properties of cast Mg-Gd-Y-Zn alloys. *Materials Science and Engineering: A*. 2017;708:482-491.

4. Chen Q, Zhao ZX, Shu DY, Zhao ZD. Microstructure and mechanical properties of AZ91D magnesium alloy prepared by compound extrusion. *Materials Science and Engineering: A*. 2011;528(10-11):3930-3934.

5. Luo A, Pekguleryuz MO. Cast magnesium alloys for elevated temperature applications. *Journal of Materials Science*. 1994;29(20):5259-5271.

6. Chen Q, Shu DY, Hu CK, Zhao ZD, Yuan BG. Grain refinement in an as-cast AZ61 magnesium alloy processed by multi-axial forging under the multitemperature processing procedure. *Materials Science and Engineering: A*. 2012;541:98-104.

7. Li YL, Wu GH, Chen AT, Jafari Nodooshan JR. Effects of Gd and Zr additions on the microstructures and high-temperature mechanical behavior of Mg-Gd-Y-Zr magnesium in the product form of a large structural casting. *Journal of Materials Research*. 2015;30(22):3461-3473.

8. Wang J, Meng J, Zhang DP, Tang DX. Effect of Y for enhanced age hardening response and mechanical properties of Mg-Gd-Y-Zr alloys. *Materials Science and Engineering: A*. 2007;456(1-2):78-84.

9. Chen Q, Shu DY, Zhao ZD, Zhao ZX, Wang YB, Yuan BG. Microstructure development and tensile mechanical properties of Mg-Zn-RE-Zr magnesium alloy. *Materials & Design*. 2012;40:488-496.

10. Honma T, Ohkubo T, Kamado S, Hono K. Effect of Zn additions on the age-hardening of Mg-2.0Gd-1.2Y-0.2Zr alloys. *Acta Materialia*. 2007;55(12):4137-4150.

11. Liu K, Zhang JH, Sun W, Qiu X, Lu HY, Tang DX, et al. Effect of Zn concentration on the microstructures and mechanical properties of extruded Mg-7Y-4Gd-0.4Zr alloys. *Journal of Materials Science*. 2009;44(1):74-83.

12. Li DJ, Zeng XQ, Dong J, Zhai CQ, Ding WJ. Microstructure evolution of Mg-10Gd-3Y-1.2Zn-0.4Zr alloy during heat-treatment at 773K. *Journal of Alloys and Compounds*. 2009;468(1-2):164-169.

13. Kawamura Y, Hayashi K, Inoue A, Masumoto T. Rapidly Solidified Powder Metallurgy Mg97-Zn1Y2 alloys with Excellent Tensile Yield Strength above 600MPa. *Materials Transactions*. 2001;42(7):1172-1176.

14. Inoue A, Kawamura A, Matsushita M, Hayashi K, Koike J. Novel hexagonal structure and ultrahigh strength of magnesium solid solution in the Mg-Zn-Y system. *Journal of Materials Research*. 2001;16(7):1894-1990.

15. Abe E, Kawamura Y, Hayashi K, Inoue A. Long-period ordered structure in a high-strength nanocrystalline Mg-1at% Zn-2at% Y alloy studied by atomic-resolution Z-contrast STEM. *Acta Materialia*. 2002;50(15):3845-3857.

16. Xu C, Zheng MY, Xu SW, Wu K, Wang ED, Kamado S, et al. Ultra high-strength Mg-Gd-Y-Zn-Zr alloy sheets processed by large-strain hot rolling and ageing. *Materials Science and Engineering: A*. 2012;547:93-98.

17. Li HZ, Liu HT, Li FB, Wang HJ, Liang XP, Liu CM. Microstructures and Properties of Extruded Mg-Gd-Y-Zr Alloys Containing Zn. *Journal of Materials Engineering and Performance*. 2012;21(6):1056-1060.

18. Zheng L, Liu CM, Jin J, Wang X, Ji DW. Effect of Hot-Rolling on Microstructures and Mechanical Properties of Extruded Mg-6Gd-3.2Y-xZn-0.5Zr Sheet. *Journal of Materials Engineering and Performance*. 2013;22(1):104-111.

19. Huang S, Wang JF, Hou F, Huang XH, Pan FS. Effect of Gd and Y contents on the microstructural evolution of long period stacking ordered phase and the corresponding mechanical properties in Mg-Gd-Y-Zn-Mn alloys. *Materials Science and Engineering: A*. 2014;612:363-370.

20. Suzuki M, Kimura T, Koike J, Maruyama K. Strengthening effect of Zn in heat resistant Mg-Y-Zn solid solution alloys. *Scripta Materialia*. 2003;48(8):997-1002.

21. Liu H, Bai J, Yan K, Yan JL, Ma AB, Jiang JH. Comparative studies on evolution behaviors of 14H LPSO precipitates in as-cast and as-extruded Mg-Y-Zn alloys during annealing at 773 K. *Materials & Design*. 2016;93:9-18.

22. Itoi T, Seimiya T, Kawamura Y, Hirohashi M. Long period stacking structures observed in Mg97Zn1Y2 alloy. *Scripta Materialia*. 2004;51(2):107-111.

23. Matsuda M, Ii S, Kawamura Y, Ikuhara Y, Nishida M. Variation of long-period stacking order structures in rapidly solidified Mg97Zn1Y2 alloy. *Materials Science and Engineering: A*. 2005;393(1-2):269-274.

24. Zheng L, Liu CM, Wan YC, Yang PW, Shu X. Microstructures and mechanical properties of Mg-10Gd-6Y-2Zn-0.6Zr(wt.%) alloy. Journal of Alloys and Compounds. 2011;509(35):8832-8839.

25. Yang Q, Xiao BL, Wang D, Zheng MY, Wu K, Ma ZY. Formation of long-period stacking ordered phase only within grains in Mg-Gd-Y-Zn-Zr casting by friction stir processing. *Journal of Alloys and Compounds*. 2013;581:585-589.

26. Zhu YM, Morton AJ, Nie JF. The 18R and 14H long-period stacking ordered structures in Mg-Y-Zn alloys. *Acta Materialia*. 2010;58(8):2936-2947.

27. Suzuki M, Kimura T, Koike J, Maruyama K. Effects of zinc on creep strength and deformation substructures in Mg-Y alloy. *Materials Science and Engineering: A*. 2004;387-389:706-709.

28. Egusa D, Abe E. The structure of long period stacking/order Mg-Zn-RE phases with extended non-stoichiometry ranges. *Acta Materialia*. 2012;60(1):166-178.

29. Yamasaki M, Matsushita M, Hagihara K, Izuno H, Abe E, Kawamura Y. Highly ordered 10H-type long-period stacking order phase in a Mg-Zn-Y ternary alloy. *Scripta Materialia*. 2014;78-79:13-16.

30. Xu DK, Liu L, Xu YB, Han EH. Effect of microstructure and texture on the mechanical properties of the as-extruded Mg-Zn-Y-Zr alloys. *Materials Science and Engineering: A*. 2007;443(1-2):248-256.